Discrete Optimal Control & Analysis of a PEM Fuel Cell Vehicle to Grid (V2G) System

Final Report
April 20th, 2007

Scott Moura
Siddhartha Shankar

ME 561 – Winter 2007
Professor Huei Peng

Abstract

Discrete optimal control methods are applied to a PEM hybrid fuel cell vehicle (HFCV) for vehicle to grid (V2G) applications. The HFCV model is developed from past control-oriented models. Grid power demand is modeled by adapting a 24-hour power forecast created by CAISO. The control problem formulation includes regulating both battery state of charge and fuel cell system efficiency. Linearization is performed about a specified operating point and the resulting transfer functions are discretized for a sampling frequency four times faster than the fastest plant dynamics. Linear systems analysis is performed on the discrete pulse transfer functions to extract physical interpretations about system dynamics. A linear quadratic regulator (LQR) and Luenberger estimator are synthesized in both continuous and discrete time to achieve the desired performance specifications. A thorough discussion on LQ weight selection is provided in addition to a presentation of several analysis tools. Observer pole placement and state estimation are analyzed with respect to disturbance rejection and error convergence. Conclusions are drawn about the effect of sampling time for the dynamic model, considering a 24-hour process disturbance cycle. To close, a summary of the salient lessons learned from the project is presented, along with recommendations for further extending this study.

Table of Contents

1. Introduction

1.1 V2G Background

The fuel cell vehicle fleet and electric power grid are remarkably complementary as systems for managing energy. Proton exchange membrane (PEM) fuel cells produce energy with nearly twice the efficiency of internal combustion engines [1]. Fuel cells also hold the potential to generate power locally and from a wide variety of energy sources. This presents an opportunity to leverage the power generating and absorbing capacity of a hybrid fuel cell vehicle (HFCV) to help load balance localized grid segments while simultaneously increasing grid stability and reliability. This concept is widely known as Vehicle to Grid (V2G). The objective of this project is to study discrete optimal control methods for regulating battery state of charge (SOC) and maximizing fuel cell system efficiency and analyze the significance of various synthesize techniques. The subsequent analysis will provide insight to the inherent trade-offs between design objectives, while elucidating characteristics unique to optimal control techniques.

1.2 Problem Statement

Hybrid energy sources have the potential to provide energy at very high efficiencies and store excess energy. However, a key obstacle to realizing these benefits exists in control system design. Our investigation seeks to analyze dynamic modeling techniques and synthesize optimal control methods for realizing optimal battery regulation and desirable fuel cell system (FCS) efficiency. First, a PEM hybrid fuel cell system (HFCS) model is discussed and each sub-model is analyzed in detail. A methodology is also developed for modeling the power grid demand for a 24 hour cycle. In the following section control system design is introduced by the mathematical problem formulation. Linearized models are created for the plant and analyzed against the original nonlinear models. The models are discretized by forming ZOH augmented pulse transfer function and analyzed with respect to zero-pole cancellations and the corresponding physical interpretations. Both continuous and discrete-time linear optimal regulators (LQR) are synthesized. The weight selection problem is discussed at length by leveraging several analysis tools used to extract physical interpretations of the control algorithm. Since it is often difficult to accurately measure dynamic states, observer pole placement is discussed within the context of designing a Luenberger estimator.

2. Nomenclature

2.1 Symbols

A	Area
e, V	Voltage
I	Current
J	LQR performance index
k	Discrete time-step
P	Power
p	Pressure
Q	Charge
q	State weight matrix component
r	Control input weight matrix component
SOC	Battery state of charge
T	Temperature
V	Voltage
W	Mass flow rate
δ	Perturbation
ω	Angular velocity
η	Efficiency
κ	Motor parameter or orifice constant
A,B,C,G,H	System matrices
K	Full-state feedback gain
L	Observer gain
Q	State weight matrix
R	Control input weight matrix
u	Control input
w	Process disturbance
x	Dynamics states
y	Measurements/Outputs

2.2 Common Subscripts

an	Anode
atm	Atmospheric
batt	Battery
dem	Demand
fcs	Fuel cell system
ca	Cathode
cp	Compressor
cm	Compressor motor
H_2	Hydrogen
in	Inlet
max	Maximum
min	Minimum
oc	Open Circuit
out	Outlet
sm	Supply manifold
st	Fuel cell stack
req	Requested
rm	Return manifold

3. PEM Hybrid Fuel Cell System Model

In order to formulate a suitable optimization problem, an analysis model is required to feed responses back to the optimization algorithm, given a set of design variables. The performance of the given set of design variables is evaluated by the optimization algorithm, which then feeds a new set of design variable back to the optimization algorithm. This iterative process continues until the optimization algorithm is able to converge to an optimal solution. This section discusses the separate subsystems that comprise the overall PEM hybrid fuel cell system model used for analysis. The optimization problem formulation is discussed in the following section.

3.1 Fuel Cell System

Accurately modeling a fuel cell system is a non-trivial process, involving considerations for the electrochemistry, hydrogen and air manifolds, membrane water content, flow control/supercharging devices, vehicle inertia dynamics, and cell/stack temperatures [2]. Clearly, preparing a mathematical systems-level model based on first principles can be a formidable task, reflected by the relative lack of publications in this area. The most widely used and studied model existing in the literature was developed in a control oriented fashion by Pukrushpan *et al.* [3]. Since the model was developed specifically for vehicle control studies, certain dynamic effects were included and others neglected, based upon the relative time constant of each phenomenon. This model has both advantages and limitations with respect to simulation accuracy and complexity. A first principles approach to system dynamics guarantees a level of validity at the cost of computational efficiency. Moreover, the model is limited in its applicability as the parameter values are based on an antiquated Ford P2000 fuel cell. Nevertheless, this model is popular among the controls community and has been shown to deliver reasonably accurate results. A summary of the principles used in the development of individual components, including the fuel cell stack, compressor, and other auxiliary components provides a general background for the system under study. Some equations are shown for simple illustration and others omitted for simplicity. The reader can refer to [3] for detailed derivations and explanations of all components and sub-models.

3.1.1 Fuel Cell Stack

The fuel cell stack model contains four interacting sub-models, including the stack voltage, anode flow, cathode flow, and membrane hydration model. The stack voltage model is comprised of an open circuit voltage and three types of losses. The open circuit voltage is computed from the energy balance between chemical energy in the reactants and electrical energy formed. The chemical reaction which takes place in the cell is given by

$$H_2 + \frac{1}{2} O_2 \rightarrow H_2 O \tag{1}$$

The energy produced can be computed by the Gibbs free energy and Nernst voltage equation. However, this only represents the so-called open circuit voltage and in reality losses occur. These losses are represented by an activation loss, ohmic loss, and concentration loss. In total, the sum of the voltage created and lost forms the cell terminal voltage, given by Equation (2). The fuel cell polarization curve shown in Figure 1 provides a visual representation of the cell voltage created with respect to current density.

$$E_{oc} - E_{act} - E_{ohm} - E_{conc} \tag{2}$$

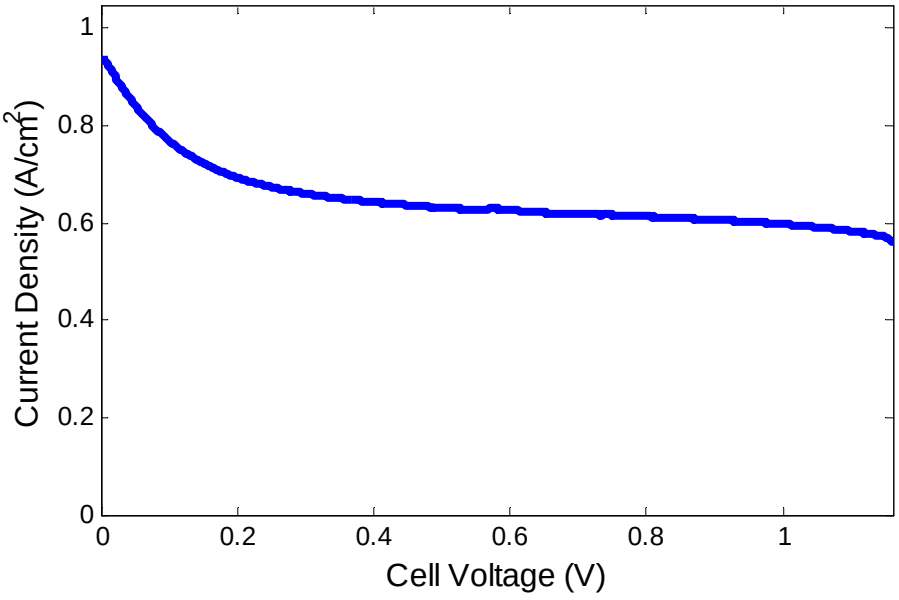

Figure 1: Fuel cell polarization curve generated from model developed in [3]

The cathode mass flow models capture the dynamic effects of air flow behavior as it enters the stack. The equations used in the development of this model use the principles of mass

conservation, thermodynamics, and psychometric properties of air. The three dynamic states within this sub-model include the masses of oxygen, nitrogen, and water vapor.

Similar to the cathode sub-model, the anode mass flow model uses the principles of mass continuity, thermodynamics, and psychometric properties. However, the anode mass flow contains hydrogen as opposed to air. The dynamics states in the anode are the masses of hydrogen and water.

A membrane hydration model serves the purpose of predicting the water content within the membrane and mass flow rate of water across the membrane. Some very significant assumptions are made, including that the mass flow is assumed to be uniform across the overall surface area of the membrane.

3.1.2 Compressor

The compressor model is separated into two components: compressor & compressor motor inertia dynamics and an efficiency map. The dynamics are modeled by a lumped rotational inertia model representing the compressor and motor masses. Applying Euler-Newton equations results in a single state given by the rotational speed of the compressor. Mass flow rate characteristics are modeled using the Jensen & Kristensen method [4]. Compressor efficiency is derived using curve fitting methods for data obtained from an Allied Signal compressor. The efficiency map takes the pressure ratio across the compressor and mass flow rate as inputs.

$$\eta_{CP} = f\left({p_{SM}}/{p_{atm}}, W_{CP} \right) \tag{3}$$

3.1.3 Auxiliary Components

The remaining auxiliary components within the model include supply manifold, return manifold, cooler, and humidifier. Both manifolds are modeled as lumped volumes associated with the pipes and connections between each device. Since the pressure difference between the supply manifold and cathode is relatively small, a linear nozzle equation approximates the mass flow rate

$$W_{SM,out} = \kappa_{SM,out}\left(p_{SM} - p_{CA}\right) \tag{4}$$

Conversely, the return manifold experiences a relatively large pressure drop between the anode and atmosphere, therefore requiring a nonlinear nozzle equation. For simplicity, the equation is omitted here, since the goal is to highlight general modeling concepts and not exact equation derivations.

Air leaving the compressor is typically very hot and may damage the MEA. Hence, a cooler is utilized to reduce incoming air temperature to fuel cell stack operating temperature, $T_{st} = 80°C$. Air flow is also humidified before entering the stack in order to ensure proper hydration of the MEA. This is performed by injecting water into the air mass flow. Simple psychometric properties and relations are leveraged to model this effect.

3.2 Battery

The battery model is adapted from the ADVISOR energy storage system model. The system comprises of a single input and two outputs. The input signal is the amount of power charged or discharged from the battery. The model outputs include SOC level and charge/discharge power limits. Numerically, positive power on the input port represents battery discharge, and conversely negative power represents battery charge. The ADVISOR battery model uses the resistive equivalent circuit model developed by the National Renewable Energy Laboratory (NREL), shown in Figure 2. This modeling framework provides sufficient fidelity of the salient battery characteristics while enabling the use of mathematical equations to model system-level performance and efficiency. Two lumped parameters, R and V_{oc} are necessary to fully describe the characteristics of the battery. These two parameters are functions of SOC level and temperature. We, however, assume isothermal operations in this study for simplicity.

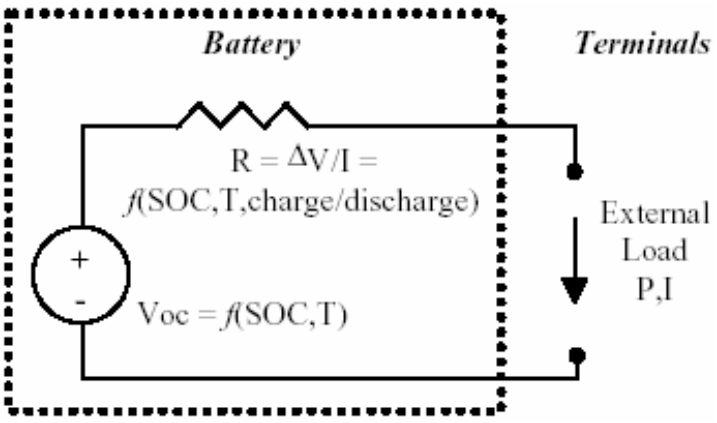

Figure 2: Resistive equivalent circuit model

The resistive equivalent circuit model leads to a set of algebraic equations, defining open circuit voltage and current through the resistor. To output SOC, current is integrated with respect to time, thus forming a first order dynamic system, as described in Equation (8). Following are the most significant equations needed for the model shown in Figure 2.

$$V_{oc} = f(SOC,T) \quad , \quad R_{\text{int}} = f(SOC,T) \tag{5}$$

$$P_{batt\_\text{lim}} = f(P_{batt\_req}, V_{oc}, R_{\text{int}}) \tag{6}$$

$$I_{batt} = -\frac{V_{oc} - \sqrt{V_{oc}^{\ 2} - 4P_{batt\_\text{lim}} R_{\text{int}}}}{2R_{\text{int}}} \tag{7}$$

$$\dot{SOC} = -\frac{I_{batt}}{Q_{\max}} \Rightarrow SOC = \frac{Q_{\max} - \int I_{batt} dt}{Q_{\max}} \tag{8}$$

Note that V and R are nonlinear functions of both SOC and temperature, forming a nonlinear map that defines the characteristics of the battery [5].

3.3 Grid Power Demand Cycle

In order to simulate a hybrid fuel cell system providing stationary power, a representative grid power demand cycle must be applied in similar fashion to using a drive cycle for mobile applications. This is accomplished by using the forecasted power demand on a typical weekday (Tuesday March 6, 2007) for the California power grid, as provided by the California Independent System Operator (CAISO). This data is easily obtained by logging onto the

CAISO website at www.caiso.com [6]. A representative figure of the data provided by CAISO is provided in Figure 3.

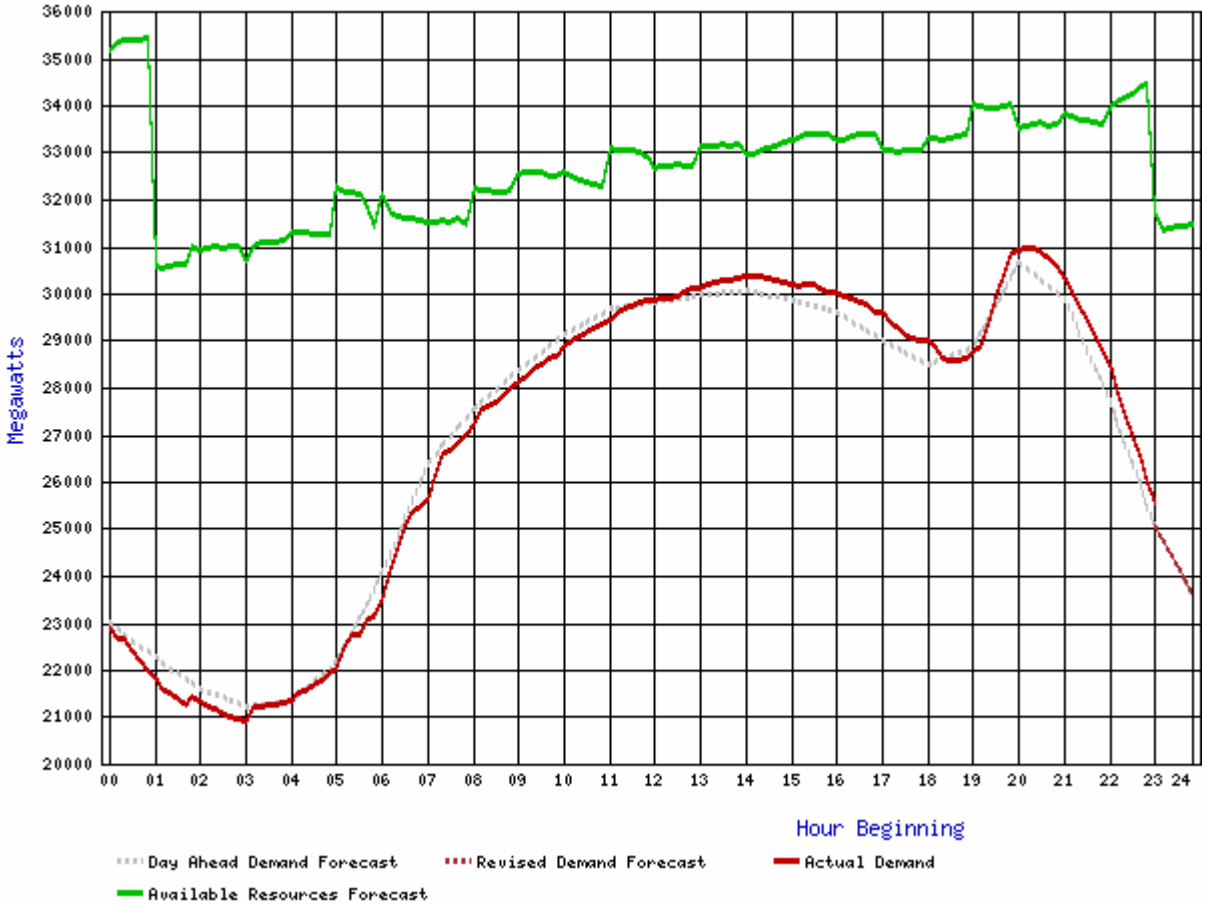

Figure 3: A single day power outlook for the California ISO control area. The forecasted power from Tuesday March 6, 2007 is utilized for development of the grid power demand cycle [9].

This data is modified in three stages to create a suitable power demand cycle. First, a continuous and smooth cycle is formed using a cubic spline on the data points. These values are then scaled down to power demand values that are on the order of magnitude for a typical office building or apartment complex. Second, a white Gaussian noise frequency distribution is superimposed on the cycle to model fast power demand changes, such as turning lights on and off, using a toaster oven, heated central air system, etc. In the third stage, the time scale is compressed from 24 hours to 720 seconds in order to create a feasible simulation time which contains the overall characteristics of a full day cycle. The resulting representative grid power demand cycle is shown in Figure 4 for a full day, from 6am to 6am.

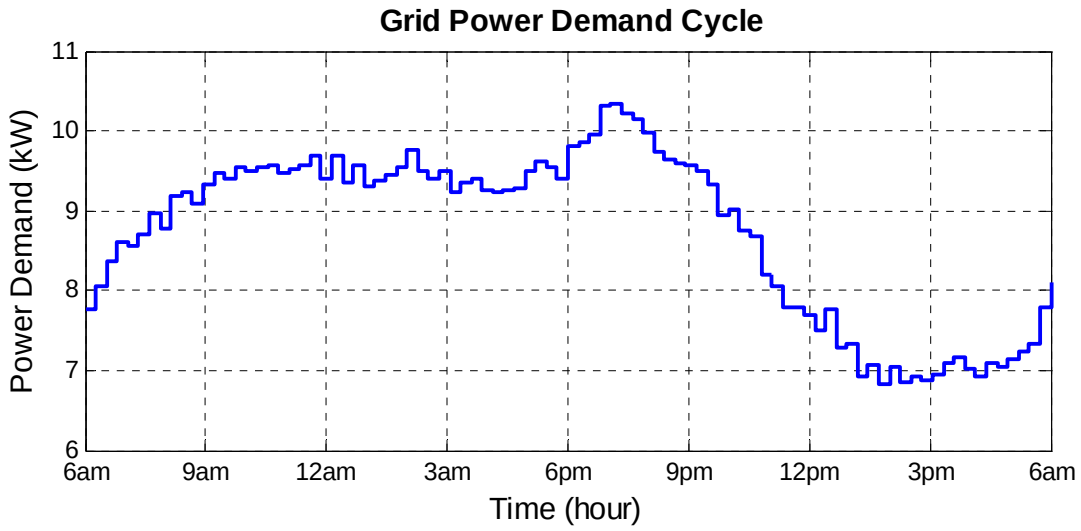

Figure 4: Scaled, splined grid power demand cycle with white Gaussian noise over 24 hour period. This cycle is compressed to 720 sec for simulation. [Source: Cal ISO Power Demand Forecast - Tuesday March 6, 2007]

4. Control Design

As discussed in the introduction and problem statement, fuel cells are capable of producing electric power at relatively high efficiency. Moreover, hybrid configurations are well suited for V2G due to their energy storage capacity. As a result, it becomes of great interest study how energy may be optimally regulated within the battery while ensuring excellent fuel cell efficiency. The following section expands on this discussion by deriving a rigorous formulation of the control problem. Subsequently, the nonlinear model is linearized about a nominal operating point, which is then verified against the original model. A discrete-time transformation is performed on the plant and the subsequent model is analyzed against its continuous-time counterpart. A linear quadratic optimal control method is synthesized for regulating battery state of charge and fuel cell efficiency, in both continuous and discrete time. Since it is very difficult to measure state of charge, a Luenberger observer is designed and the closed loop system is analyzed.

4.1 Control Problem Formulation

The control design objective is to synthesize a control algorithm to regulate battery SOC while retaining desirable fuel cell system performance, while rejecting process disturbances represented by power demand from the grid. The control inputs to the plant include fuel cell

stack current, I_{st}, and compressor motor voltage, e_{cm}. The hybrid fuel cell system provides power to the electric grid, which can be modeled as a process disturbance to the plant, given by P_{grid}. As discussed in Sections 3.1 and 3.2, the model states include compressor inertia speed and supply manifold pressure for the fuel cells system, and electric charge consumed by the battery. Recall that electric charge consumed is algebraically related to SOC, and therefore considered equivalent in terms of dynamic response. The measurable outputs of the system include the battery's open circuit voltage, V_{oc}, and fuel cell system efficiency (including parasitic losses by the compressor), η_{fcs}. The inputs, disturbances, outputs, and states are represented in mathematical vector form by Equation (9).

$$\mathbf{u} = \begin{bmatrix} I_{st} \\ e_{cm} \end{bmatrix} \quad \mathbf{w} = P_{grid} \quad \mathbf{x} = \begin{bmatrix} \omega_{cp} \\ p_{sm} \\ Q_{used} \end{bmatrix} \quad \mathbf{y} = \begin{bmatrix} V_{oc} \\ \eta_{fc} \end{bmatrix} \tag{9}$$

To synthesize a closed loop feedback control system with desirable dynamic characteristics, the pole placement method known as full-state feedback is employed. Full-state feedback uses information about the states to compute the appropriate control inputs that achieve the desired response. Although a very simple and powerful method, this control formulation requires knowledge of the state variables, which may be impractical or even impossible. Therefore, a Luenberger observer is applied to estimate values for the states, $\hat{\mathbf{x}}$, which are fed to the full-state feedback gain, $\mathbf{K}$. Due to the principle of separation for an observer-based compensator, the full-state feedback and observer are synthesized independently. The closed-loop control system is schematically given by the block diagram in Figure 5.

The two control objectives are to regulate SOC to a value of 0.7 and achieve desirable fuel cell system efficiency characteristics. Intuitively, regulating SOC is most effectively performed by applying high energy control action. However, this likely decreases fuel cell system efficiency. This tradeoff is discussed at length throughout the controller synthesis process.

Scott Moura
Siddhartha Shankar

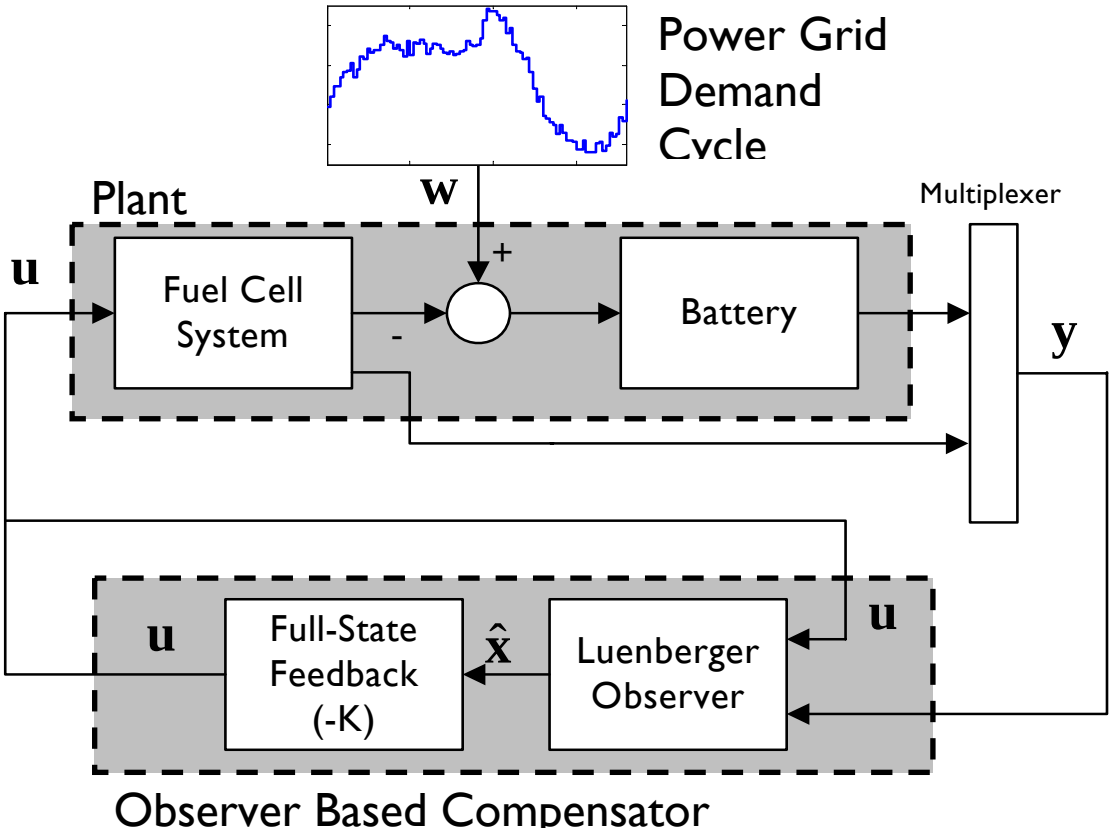

Figure 5: Block diagram representation of closed-loop control system, including plant, disturbance, and observer based compensator.

4.2 Linearization

The nonlinear model developed by the authors of [7] is linearized in continuous-time using the Simulink® Control Design interface in MATLAB. The nominal operating points are chosen by selecting the average values for each state when constant control inputs are provided along with the power demand cycle shown above. The nominal operating points are denoted by a superscript 0 and given by Equation (10).

$$\mathbf{u}^0 = \begin{bmatrix} 30A \\ 42.6V \end{bmatrix} \quad \mathbf{w}^0 = 8500W \quad \mathbf{x}^0 = \begin{bmatrix} 2646\frac{rad}{\text{sec}} \\ 111{,}570Pa \\ 1.8C \end{bmatrix} \quad \mathbf{y}^0 = \begin{bmatrix} 155.331V \\ 0.5892 \end{bmatrix} \tag{10}$$

The linearized model is derived in continuous-time and represented by perturbation variables, as shown in Equation (11):

$$\begin{aligned} \delta\dot{\mathbf{x}} &= \mathbf{A}\delta\mathbf{x} + \mathbf{B}\delta\mathbf{y} + \mathbf{G}\delta\mathbf{w} \\ \delta\mathbf{y} &= \mathbf{C}\delta\mathbf{x} + \mathbf{D}\delta\mathbf{y} + \mathbf{H}\delta\mathbf{w} \end{aligned} \tag{11}$$

where $\delta(\bullet) = (\bullet) - (\bullet)^0$ represents the perturbation about the nominal operating point [3]. Note that the use of perturbation variables provides a convenient transformation in which the origin of the perturbed system represents the operating point about which linearization is performed. This dynamic system realization has convenient properties for regulating performance variables by minimizing their perturbation about the operating point.

To verify the accuracy of the linearized model near the nominal operating point, sinusoidal control inputs and the power demand cycle described in Section 3.3 are applied to both the original and linearized systems. Figure 6 depicts the output responses for both models, where it is clearly noted that the linearized model does a reasonable good job of approximating the original nonlinear model. By utilizing a linearized model, all the tools for linear system analysis and design become available. The following section leverages these techniques to discuss significant characteristics of the dynamic model.

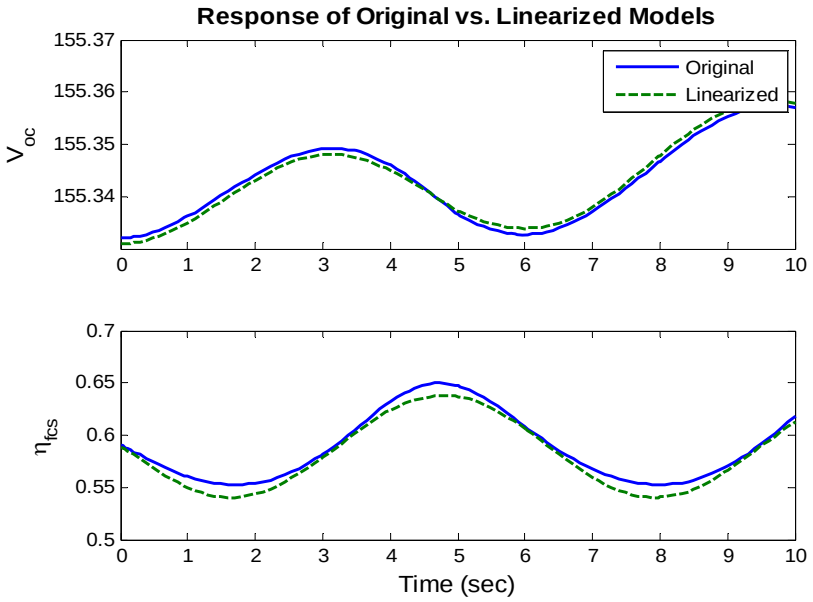

Figure 6: Response of original vs. linearized model for sinusoidal control inputs and power demand cycle disturbance.

4.3 Discrete System Analysis and Design

4.3.1 Continuous to Discrete Transformation of Plant

The linearized fuel cell-battery plant model was converted to a Zero Order Hold (ZOH) equivalent pulse transfer function using a sampling time of 0.05 seconds. The sampling time was selected based on the value of the fastest pole in the continuous time system (i.e. the system is sampled at a rate four times faster than the fastest dynamics in the plant). For the 3-input/2-output system representing our plant, Table 1 gives the discrete time transfer functions of each input-output pair.

		Output	
		Open Circuit Voltage	*FCS Efficiency*
Input	*Stack Current*	$\frac{2.79\times10^{-5}(z-0.768)(z-0.212)}{(z-1)(z-0.7678)(z-0.2087)}$	$\frac{-0.0033(z-1)(z-0.766)(z-0.203)}{(z-1)(z-0.7678)(z-0.2087)}$
	CM Voltage	$\frac{1.81\times10^{-8}(z+2.48)(z+0.16)}{(z-1)(z-0.7678)(z-0.2087)}$	$\frac{2.80\times10^{-5}(z-1)(z+0.55)}{(z-1)(z-0.7678)(z-0.2087)}$
	Power Demand Cycle	$-\frac{-1.16\times10^{-7}(z-0.77)(z-0.21)}{(z-1)(z-0.7678)(z-0.2087)}$	0

Table 1: Discrete-time transfer functions for MIMO system using a sampling time of T = 0.05s.

4.4 Linear Quadratic Regulator

The primary objective of the control system design is to regulate state of charge by controlling the open circuit voltage of the battery. The secondary objective is to select parameters for this design that also ensures that the fuel-cell operates in an "optimal region" which maximizes fuel cell efficiency.

A linear quadratic regulator (LQR) is well suited for a control problem in which we wish to penalize deviations from a nominal operating point. Computationally, this technique computes the optimal control law $\mathbf{u}^* = -\mathbf{K}^*\mathbf{x}$ so that the following performance index, in continuous or discrete time, is minimized:

$$J = \int_0^\infty \left[\mathbf{x}^{\mathbf{T}}(t)\mathbf{Q}\mathbf{x}(t) + \mathbf{u}^{\mathbf{T}}(t)\mathbf{R}\mathbf{u}(t)\right]dt \qquad J = \frac{1}{2}\sum_{i=0}^{\infty}\left[\mathbf{x}^{T}(i)\mathbf{Q}\mathbf{x}(i) + \mathbf{u}^{T}(i)\mathbf{R}\mathbf{u}(i)\right] \quad (12)$$

Where, $\mathbf{Q}$ and $\mathbf{R}$ are weighting matrix parameters that must be positive semi-definite and positive-definite, respectively [8]. The purpose of the matrices Q and R is to penalize deviations of the states and control inputs from their nominal operating points (usually zero for a system defined using perturbation variables). Picking the weighting matrix components is a primary challenge of the optimal control design process. A discussion of weights selected is provided in Section 5.2. The process of picking weights is by itself iterative in nature. However, once an initial set of weights yielding somewhat satisfactory performance are identified, they are further tuned to give the level of performance desired.

The solution to the algebraic Riccatti equation yields the optimal full-state feedback gain $\mathbf{K}^*$, derived in both discrete and continuous time. Figure 7 presents the stack current control input (I_{st}) state of charge (SOC) and fuel cell system efficiency (η_{FCS}) time trajectories using the power demand cycle described in Section 3.3. Three plots are produced for each variable, one for the continuous time system and two for the discrete time system sampled at 0.05 seconds and 5 seconds respectively.

Clearly, each trajectory performs superbly with respect to regulating stack current, SOC, and efficiency. To illustrate the robustness of this methodology, a admittedly large 5 second sampling time is selected to compare against the continuous time solution. While good system performance for a 5 second sampling time may seem counter-intuitive, it is not wholly unexpected since battery SOC has an extremely slow Eigen-frequency. This result remains true even when power demand fluctuations are somewhat significant.

Scott Moura
Siddhartha Shankar

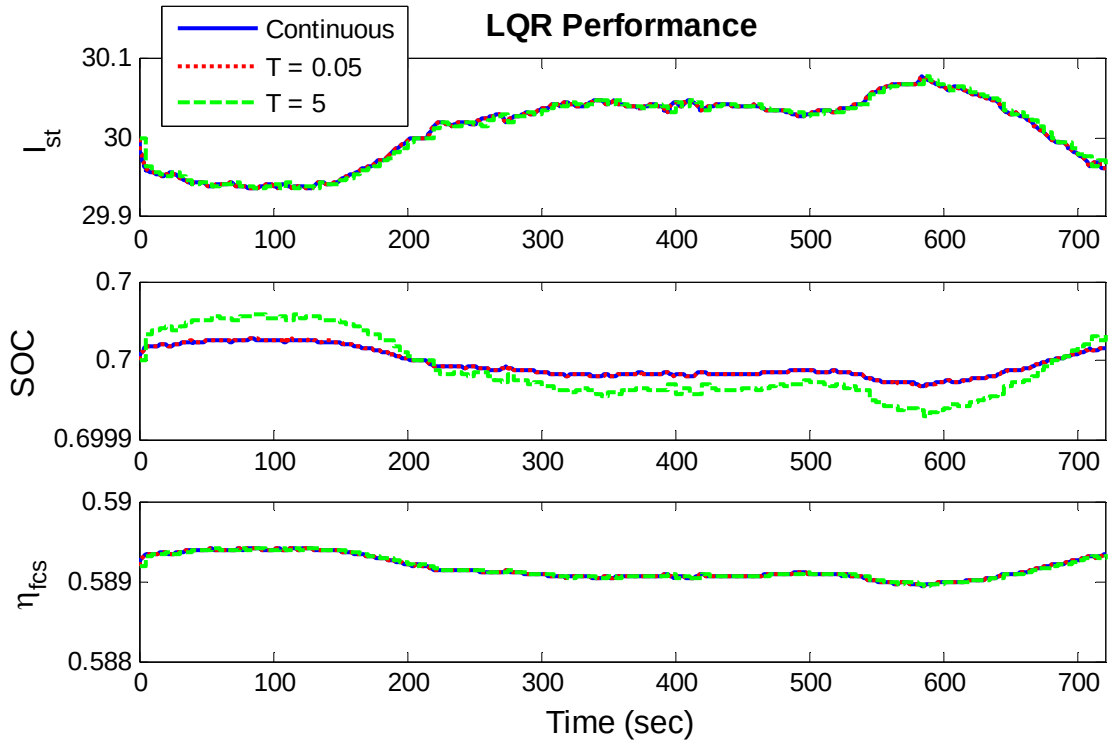

Figure 7: Control and performance variable trajectories for both continuous & discrete time LQR.

4.5 Luenberger Estimator Design

Although the battery model implemented in Simulink® is capable of numerically producing state of charge as an output, state of charge is practically inferred by measuring open circuit voltage (V_{oc}), which is directly correlated to state of charge [9]. Hence, it is of practical importance to analyze and design a full order Luenberger estimator. Consider the closed loop dynamics of the full-state feedback system, given in both continuous and discrete time by

$$\dot{\mathbf{x}} = (\mathbf{A} - \mathbf{BK})\mathbf{x} \qquad \mathbf{x}(k+1) = (\mathbf{A} - \mathbf{BK})\mathbf{x} \tag{13}$$

The estimator poles are selected such that the estimator dynamics are faster than the closed-loop dynamics. One simple method for observer pole placement is to simply scale the poles of the closed-loop system. Following a general rule off thumb, the observer poles are selected to be three times faster than the closed loop dynamics. For the continuous time case, this process is applied in a straightforward manner by multiplying the eigenvalues of the closed loop system by three.

$$\mathbf{p}_{observer} = 3 \cdot eig(\mathbf{A} - \mathbf{BK}) \tag{14}$$

For the discrete time case, the following approach is applied: By the definition of the z-transform

$$z = e^{sT} \tag{15}$$

It is desired to place poles in the z-domain that are three times faster than the closed-loop poles of the discrete system. In the s-domain, the required poles are computed by

$$p_{observer}(s) = 3 \cdot s$$

Applying the z-transform definition:

$$\begin{aligned} p_{observer}(s) &= e^{3sT} = \left(e^{sT}\right)^3 \\ p_{observer}(z) &= z^3 \end{aligned} \tag{16}$$

Hence, estimator poles which are three times faster than the closed loop dynamics in continuous time is equivalent to cubing the pole values in discrete time. The hybrid fuel cell system under consideration has closed loop poles at $\left(1.738\times10^{-6}, -5.285, -31.337\right)$ for the continuous time system and $\left(0.209, 0.768, 0.999\right)$ for the discrete time system. A Luenberger observer for is designed with closed loop poles at $\left(-5.213\times10^{-6}, -15.854, -94.013\right)$ and

	Continuous Time	**Discrete Time**
Closed-loop poles	$\left(1.738\times10^{-6}, -5.285, -31.337\right)$	$\left(0.209, 0.768, 0.999\right)$
Observer poles	$\left(-5.213\times10^{-6}, -15.854, -94.013\right)$	$\left(0.009, 0.453, 0.950\right)$

An observer computes the state estimate $\hat{\mathbf{x}}$ such that the control law $\mathbf{u} = -\mathbf{K}\hat{\mathbf{x}}$ retains similar closed loop properties as the system with full state feedback. The state estimator designed takes the form:

$$\dot{\hat{\mathbf{x}}}(t) = (\mathbf{A} - \mathbf{LC})\hat{\mathbf{x}}(t) + \mathbf{L}\mathbf{y}(t) + \mathbf{B}\mathbf{u}(t) \qquad \hat{\mathbf{x}}(k+1) = (\mathbf{A} - \mathbf{LC})\hat{\mathbf{x}}(k) + \mathbf{L}\mathbf{y}(k) + \mathbf{B}\mathbf{u}(k) \tag{17}$$

assuming there are no direct feed-forward terms.

The resultant closed loop dynamics are

$$\begin{bmatrix} \dot{\mathbf{x}}(t) \\ \dot{\tilde{\mathbf{x}}}(t) \end{bmatrix} = \begin{bmatrix} \mathbf{A} - \mathbf{BK} & \mathbf{BK} \\ \mathbf{0} & \mathbf{A} - \mathbf{LC} \end{bmatrix} \begin{bmatrix} \mathbf{x}(t) \\ \tilde{\mathbf{x}}(t) \end{bmatrix} \qquad \begin{bmatrix} \mathbf{x}(k+1) \\ \tilde{\mathbf{x}}(k+1) \end{bmatrix} = \begin{bmatrix} \mathbf{A} - \mathbf{BK} & \mathbf{BK} \\ \mathbf{0} & \mathbf{A} - \mathbf{LC} \end{bmatrix} \begin{bmatrix} \mathbf{x}(k) \\ \tilde{\mathbf{x}}(k) \end{bmatrix} \tag{18}$$

The decoupling of the estimated states $\hat{\mathbf{x}}$ from the actual states allows us to assign the closed loop poles of the measured states and the estimated states independently, due to the block

triangular form of the system matrix. Simulation results showing the convergence of observer estimated states with actual state values are shown in Section 5.3.

5. Discussion of Results

5.1 Open Loop System Analysis

Several interesting observations about the plant can be made by simply observing the transfer functions in zero-pole gain form, given previously in Table 1. Almost all transfer functions are characterized by near or exact zero-pole cancellations. This greatly reduces the initial complexity of the system and provides a more meaningful understand of the underlying dynamics. If these cancellations are removed, the approximate transfer functions reduce to forms given in Table 2.

		Output	
		Open Circuit Voltage	*FCS Efficiency*
Input	*Stack Current*	$\approx \frac{2.79\times10^{-5}}{(z-1)}$	≈ -0.0033
	CM Voltage	$\approx \frac{1.81\times10^{-8}(z+2.48)(z+0.16)}{(z-1)(z-0.7678)(z-0.2087)}$	$\approx \frac{2.80\times10^{-5}(z+0.55)}{(z-0.7678)(z-0.2087)}$
	Power Demand Cycle	$\approx \frac{-1.16\times10^{-7}}{(z-1)}$	0

Table 2: Approximate discrete-time transfer functions after near or exact zero-pole cancellations.

5.1.1 Open Circuit Voltage

Open circuit voltage is roughly the integral of stack current and power demand cycle, with a very small gain. Intuitively, this may be verified by realizing open circuit voltage has a one-to-one relationship between SOC. Therefore, the battery is modeled approximately by an integrator, i.e. a capacitive element. In the frequency domain, an integrator may be interpreted as having zero bandwidth and constant phase lag of 90°. Bode frequency response plots of these transfer functions, shown in Figure 8, confirm this suspicion. In both cases the bandwidth is equal to 1.734×10^{-6} and phase lag is almost uniformly equal to 90°. Note that the transfer function from power demand cycle to open circuit voltage has a negative sign to give phase lead in the Figure 8(b).

Scott Moura
Siddhartha Shankar

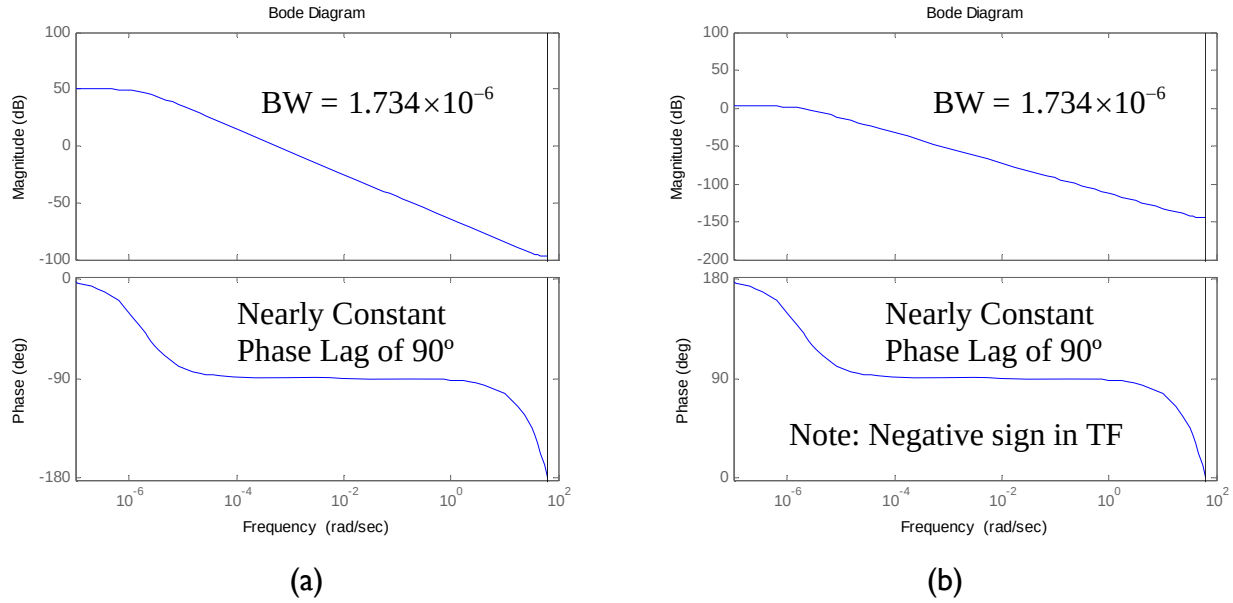

Figure 8: Frequency responses of (a) stack current & (b) power demand cycle to open circuit voltage.

5.1.2 FCS Efficiency & Stack Current

Fuel cell system efficiency is proportional to stack current, with no dynamics involved. The justification for this result is obtained by considering how fuel cell system efficiency is computed. Fuel cell system efficiency is given by the ratio of electric power produced to the thermal energy of hydrogen entering the stack.

$$\eta_{fcs} = \frac{P_{fcs,net}}{LHV \cdot \dot{m}_{H_2}} \tag{19}$$

Note that fuel cell system power is the net difference between stack power produced and compressor motor power consumed. However, our simplified model assumes the parasitic losses due to the compressor motor are zero, so $P_{fcs,net}$ reduces to stack current times stack voltage. Stack voltage is also approximately proportional to stack current, forming an estimate of net power given by Equation (20).

$$P_{fcs,net} = P_{fc} - P_{cm} = I_{st}V_{st} - P_{cm} \approx I_{st}V_{st} \approx K_1 I_{st}^{\ 2} \tag{20}$$

Mass flow rate of hydrogen consumed is exactly proportional to stack current by the number of cells in the stack, Faraday's constant and molar mass of hydrogen.

$$\text{where, } LHV \cdot \dot{m}_{H_2} = K_2 I_{st} \tag{21}$$

Combining the approximations, fuel cell system efficiency is shown to be proportional to stack current.

$$\eta_{fcs} \approx KI_{st} \tag{22}$$

Discrete time frequency response analysis provides additional insight and verification of the aforementioned arguments. Notably, a transfer function approximated by a negative gain has a gain margin equal to the Nyquist frequency and constant 180° phase lag (or lead), as illustrated by Figure 9.

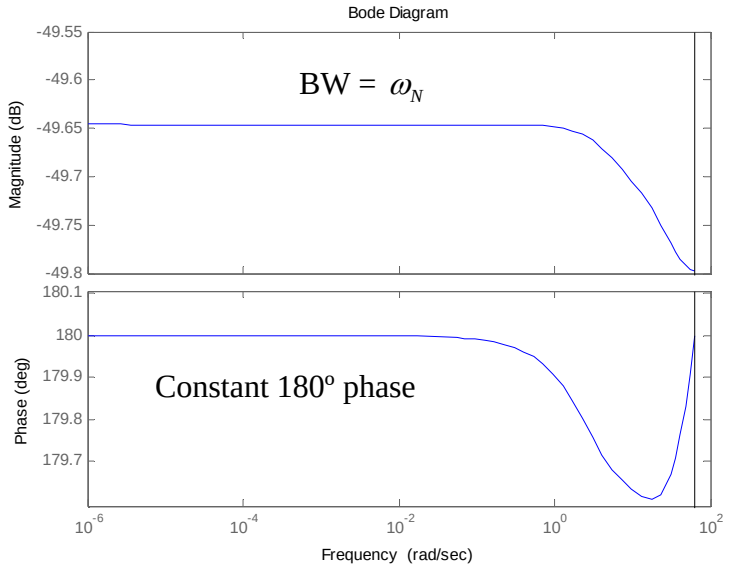

Figure 9: Frequency responses of stack current to fuel cell system efficiency.

5.1.3 FCS Efficiency & Power Demand Cycle

Power demand cycle disturbance input has no effect on FCS efficiency. This result is expected and verified by referring back to the block diagram representation in Figure 5. Recall that the power demand cycle serves as a disturbance input to the battery, downstream of the fuel cell system. If the loop is closed, however, the power demand cycle will impact FCS efficiency by way of the controller.

5.2 Linear Quadratic Weight Selection

As was discussed in Section 4.4, one method for weight selection is to find an initial value with reasonable performance and then iterate about this value to achieve satisfactory closed-loop

system responses. For the problem under investigation, the objectives are to maintain state of charge and fuel cell system efficiency subject to various constraints:

- Steady state open circuit voltage must be achieved within 1 minute
- Ensure that fuel cell operates at "optimal" efficiency for as long as possible
- Stack current must be maintained within limits (0 to 310A) i.e. control action can not be arbitrarily large and enforcing these constraints ensures that the fuel-cell is not over-utilized or damaged.

In complying to the positive semi-definite and positive definite requirements, $\mathbf{Q}$ and $\mathbf{R}$ matrices are chosen in the following diagonal form:

$$\mathbf{Q} = \begin{bmatrix} q_1 & 0 & 0 \\ 0 & q_2 & 0 \\ 0 & 0 & q_3 \end{bmatrix} \quad \mathbf{R} = \begin{bmatrix} r_1 & 0 \\ 0 & r_2 \end{bmatrix} \tag{23}$$

where q_1, q_2, q_3, r_1, r_2 correspond to the relative importance of compressor speed, supply manifold pressure, battery charge used, stack current, and compressor motor voltage, respectively. The methodology employed for selecting each parameter is the following: Chose $q_1 = q_2 = 0$ since there is no desire to regulate compressor speed or supply manifold pressure. Select $r_2 = 1$ as a nominal value for regulating compressor motor voltage. The remaining parameters, q_3 and r_1, place weights on Q_{used} and I_{st} which correspond directly to the performance variables, SOC and η_{fcs}. These two parameters are selected by managing the tradeoff between average fuel cell system efficiency and SOC rise time.

One method for analyzing the implications of weighting matrix selection is to set one parameter to a nominal value and vary the other while observing the system responses. Consider a nominal value of $r_1 = 1$ while performing a parameter sweep through a broad range of values for q_3. For each iteration, an LQR controller and corresponding feedback gain $\mathbf{K}$ are designed and various performance indices, such as open circuit voltage (one-to-one relation with SOC), stack current, efficiency and the compressor motor voltage, are monitored. The results of this iterative analysis are shown in Figure 10. A large value for q_3 places supreme importance on regulating SOC, which is represented by extremely fast rise time for V_{oc}.

However, placing such an extreme importance on SOC requires a large control input, which may exceed the 310A constraint limit. Alternatively, selecting q_3 that minimizes controller input sacrifices controller speed, which may be undesirable. Using this form of analysis, the tradeoff becomes very clear and a balance between design objectives must be negotiated carefully. Values of q_3 between 10^5 and 10^6 yield a suitably fast settling time for open circuit battery voltage, do not cause large deviations in stack current, attain optimal efficiency reasonably quickly and yield practical values for compressor motor voltage. Therefore, a value of $q_3 = 3.1623\times10^5$ is utilized throughout the remainder of this report.

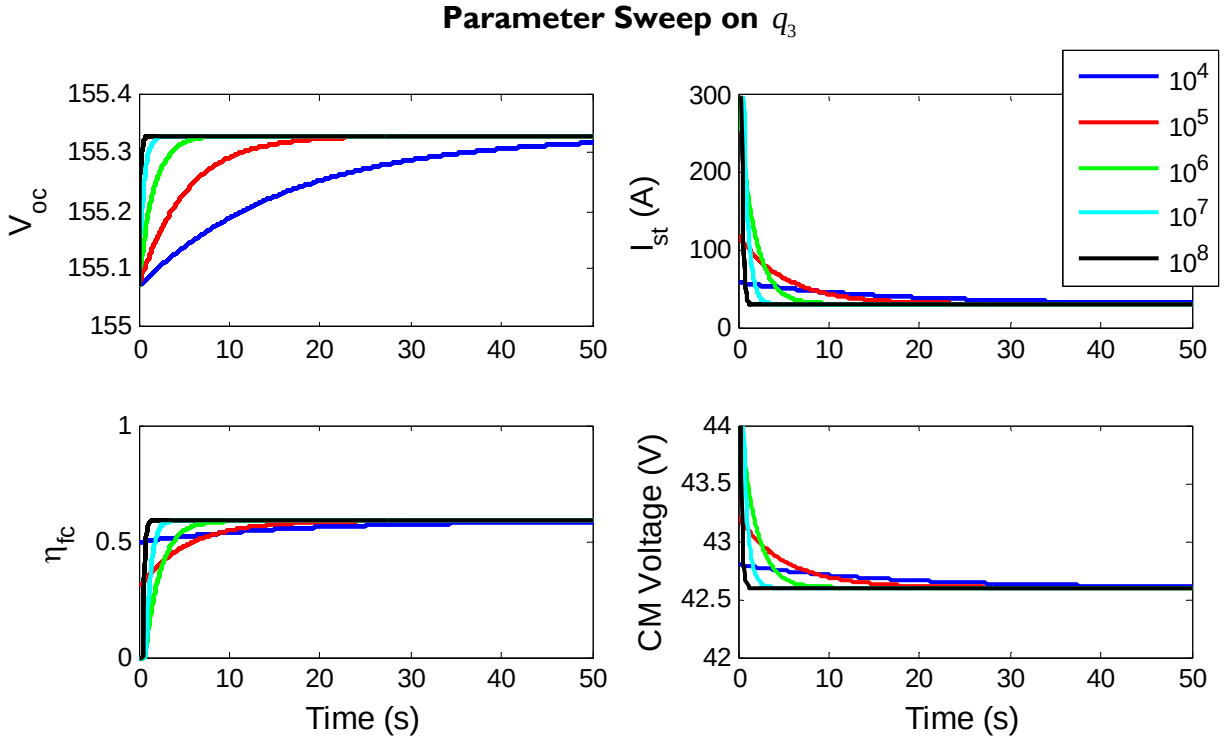

Figure 30: Weight parameter sweep on q_3 with r_1 = 1

Maintaining $q_3 = 3.1623\times10^5$, a parameter sweep is performed for r_1, in logarithmic steps. The four performance indices for each value of r_1 are given in Figure 11. Large r_1 corresponds to increased preference on regulating stack current, which is approximately proportional to FCS efficiency. However, the V_{oc} (and SOC) response is characterized by an extremely slow rise time. Selecting a small value of r_1 has the converse effect. A value of r_1 near 0.5 yields the

Scott Moura
Siddhartha Shankar

desirable performance characteristics which appears to reasonably balance each design goal. Therefore, $r_1 = 0.5$ will be used for the remainder of the design process.

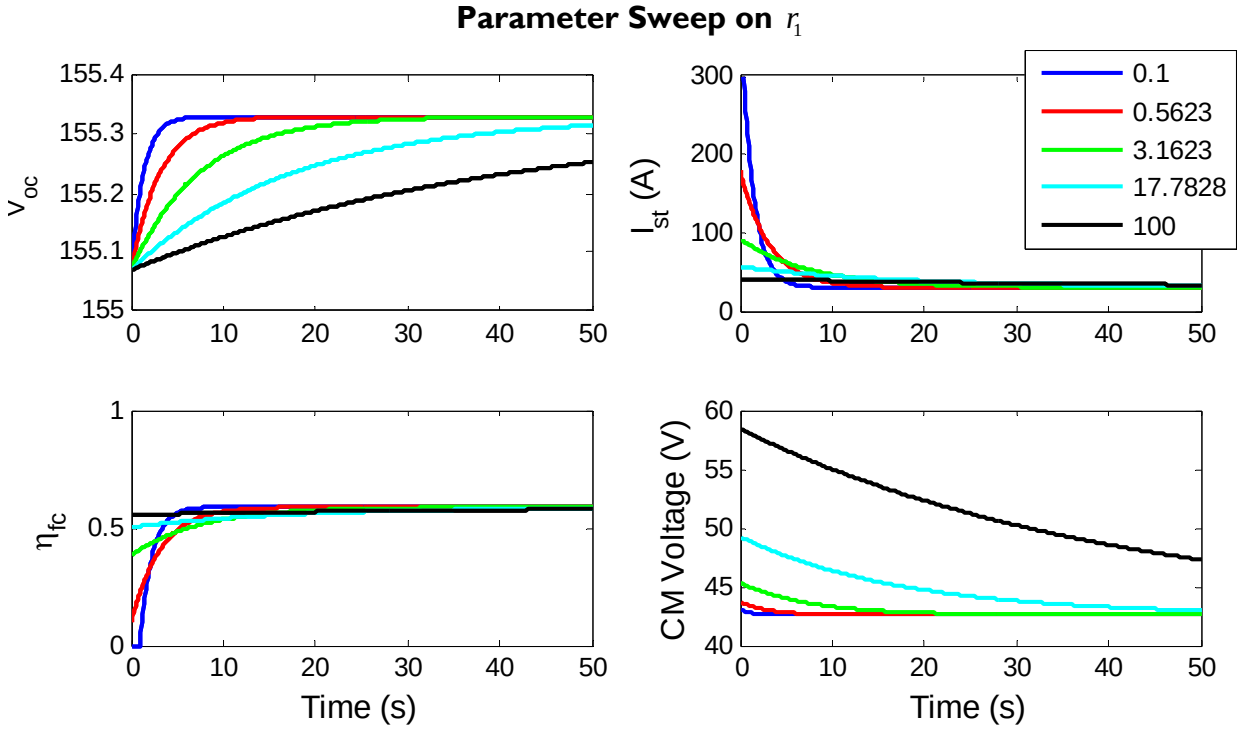

Figure 41: Weight parameter sweep on r_1 with $q_3 = 3.1623 \times 10^5$

Although simple, this sequential method of weight selection only analyzes single-dimensional subspaces at a time. An alternative method, which is easily visualized for a two dimensional design space, is to vary both weighting parameters together and create a three dimensional surface response. The two responses include FCS efficiency and SOC rise time as functions of the two weight parameters, q_3 and r_1. Using these graphs, it becomes evident that a small value of q_3 and large value for r_1 would yield high efficiency, but rise time deteriorates. Conversely, a large value of q_3 and small value for r_1 would yield fast rise time, but poor efficiency.

Scott Moura
Siddhartha Shankar

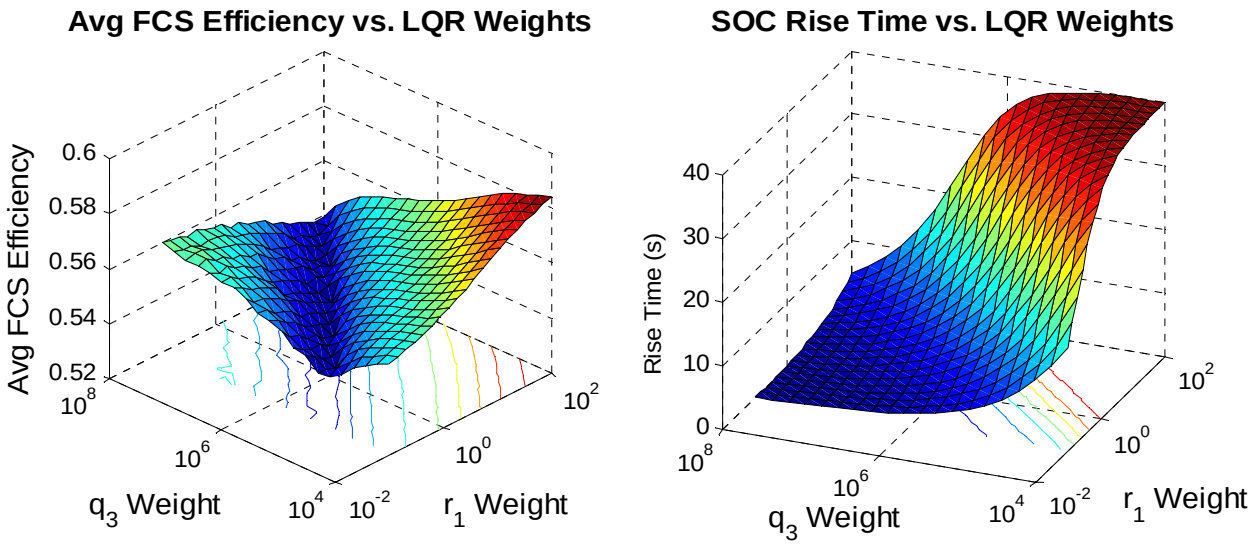

Figure 52: Average FCS efficiency and SOC rise time responses for combined weight parameter analysis

Intuitively, it is very clear that putting preference on one objective sacrifices the other. In optimization theory, this problem is known as a competing multi-objective optimization, often visualized using a Pareto Front, shown in Figure 13. Each axis corresponds to one of the objectives and the cloud of points represents optimal solutions. Note that SOC rise time is bounded by the 310A maximum stack current constraint. The points shown in blue represent feasible controllable points, whereas red signifies uncontrollable designs in which the maximum stack current exceeds 310A. Ideally the optimal solution approaches the origin, but the competing objective functions and design constraints define a boundary of feasibility which excludes the origin.

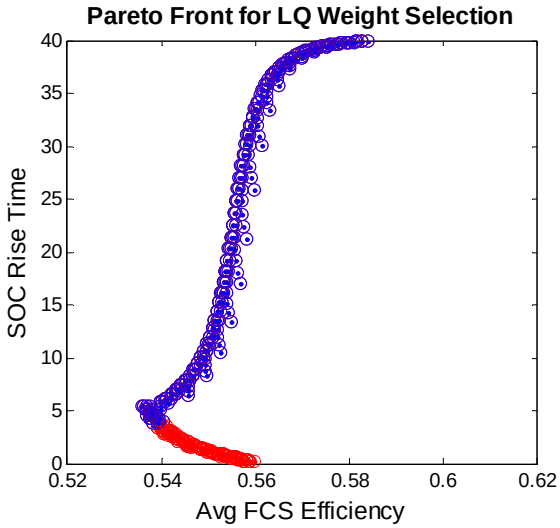

Figure 63: Pareto Front representation of LQ weight selection problem.

5.3 Observer Pole Placement

In Section 4.5, observer design is discussed in terms of placing poles to achieve the desired system dynamics. However, the selection of observer poles by itself is not straightforward and requires one to take into consideration the performance requirements and nature of the system.

One of the primary concerns while designing an observer is to ensure that the estimation error decays rapidly. Theoretically, this corresponds to picking fast poles located at the far left of the s-plane for the continuous time system or close to the origin in the z-plane for the discrete time system. While this might yield excellent results in simulations on an ideal model, practically, the presence of sensor noise will be magnified in direct proportion to the speed of the observer poles. Picking very fast poles for the observer might therefore only be feasible when one has perfect sensors and/or is working in a noise-free environment. Therefore, while selecting the observer poles, one must carefully consider the tradeoff between fast response speed and immunity to sensor noise.

Another concern in observer design is the transient performance of the observer. Selecting poles that are extremely fast could result in large transient errors which will take more time to decay. Extremely large transients due to system instabilities or the occurrence of disturbances could cause numerical errors in the observer. In a sense, the transient error of the observer is roughly proportional to $\left(|\lambda|_{\max}\right)^{n-1}$, where $|\lambda|_{\max}$ is the magnitude of the largest eigenvalue. Clearly we see that observer pole-placement is not simply a matter of picking the fastest poles, and it must be done with a consideration of the nature of the system states as well as the order of the system [10].

5.4 Estimation Analysis

The closed-loop system with observer based compensator is evaluated for satisfactory performance by applying a scaled version of the original power grid profile discussed in Section 3.3. Scaling the process input to small deviations about the linearization point is necessary to ensure the linearization assumption is satisfied.

The observer pole locations were first placed at 3x [speed of the closed loop system poles] and then at 10x [speed of closed loop system poles]. The rate of decay of estimation error was monitored for these two different observers. As discussed in the previous section, faster observer poles led to faster estimation error decay as shown in Figure 14. Not only do the estimates of the states have a lower error percentage for the faster poles, but they also converge on the actual state variables quicker and track them well thereafter. Clearly, the same can not be said for the slower observer. Although it would have been useful to have simulations showing the deterioration of performance for estimators with fast poles, that objective is left for future work.

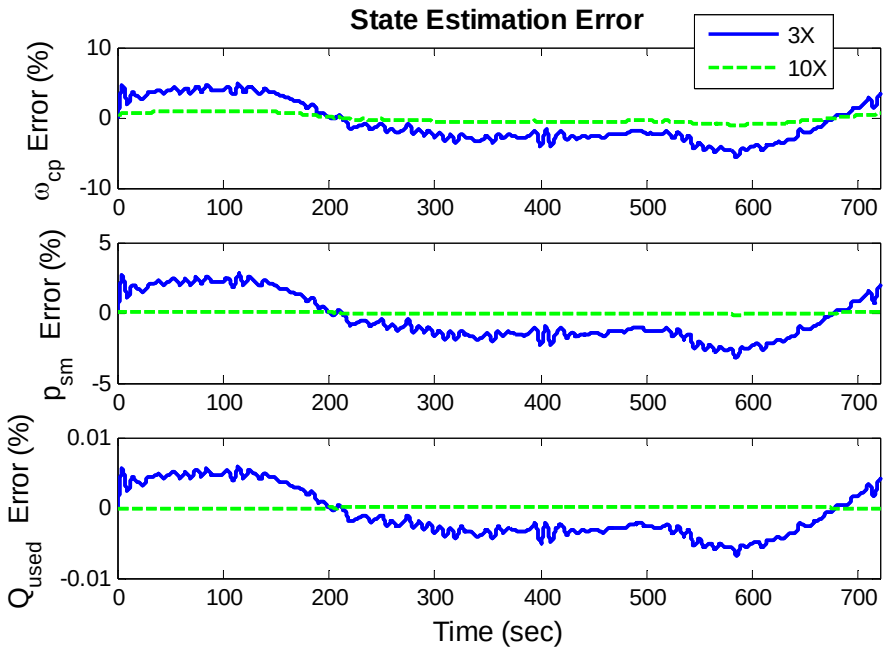

Figure 74: State estimation error for closed loop system with observer based compensator.

6. Lessons Learned

Finally, in the analysis of non-linear systems and their linearized counterparts, it was realized that one could often extract useful information about the underlying nature of the system and it's behavior by making certain simplifying assumptions on the mathematical model. For example, identifying pole-zero cancellation in a transfer function yielding a simplified form that is easier to analyze. Performing such simplifications, one could look at a battery as simply being an

integrator of charge or the fuel cell system as a gain between the input stack current and the output power.

The process of selecting weights for designing LQR optimal control was studied in depth. Various methodologies were examined and developed for selecting weights, determining tradeoffs, and formulating analysis tools.

The nuances of observer design were elucidating by applying process disturbances. The simplistic view of observer design (to simply pick the fastest possible poles) was qualified juxtaposed against a more holistic method which considers process disturbances. For example, it was determined that one should not select fast poles for the observer when the sensor measurements are known to be noisy or the system is subjected to large disturbances.

In the process of linearizing a non-linear plant about certain operating points, it was found that one must necessarily have a contingency plan in place to handle situations where control inputs or system states stray far from the operating points.

In selecting a sampling time for discrete time control systems, it was felt that focusing on the presence of fast system dynamics (if any) might not always be necessary. If a system tends to operate in a certain range of operating points and does not show too much variation, undersampling the system would not cause any problems.

It was understood that the "optimal solution" was subjective in nature and always necessitated making tradeoffs when multiple objectives are considered.

7. Recommendations

The high level of nonlinearity with respect to the power demand cycle produced a formidable challenge in control system design. As discussed previously, scaling the process disturbance to deviate by only small changes from the nominal operating point is a patchwork solution employed to facilitate a simpler control design process. This quick fix is clearly not possible in reality. Therefore, we recommend the concept of gain scheduling be applied to formulate a

family of linearized plants and corresponding controllers. As the power input from the grid varies along its highly nonlinear trajectory, a switching scheme may be employed to transition from one controller to another. This technique provides a logical and extremely practical extension to the work proposed in this paper.

An observer design that sufficiently served the purpose of estimating states was synthesized in this project. However, the observer was completed for a linear system subject to moderate process disturbances and no measurement noise. Therefore, we recommend the design of a Kalman estimator that exhibits good performance in the presence of input or output disturbances, nonlinearities, parameter perturbations in the plant and/or sensor noise.

8. Acknowledgements

We wish to acknowledge the guidance of Professor Heui Peng in helping us formulate our problem and analyze results. We also greatly appreciate Dongsuk Kum for helping us understand the nuances of LQ methods, observer design, and linear systems. Dr. Hosam Fathy & Professor Jessy Grizzle also helped us formulate ideas for the project.

9. References

[1] L. D. Burns, J. B. McCormick and C. E. Borroni-Bird, "Vehicle of change," *Sci. Am.,* vol. 287, pp. 64-73, 2002.

[2] L. Guzzella. Control oriented modelling of fuel-cell based vehicles. Presentation in NSF Workshop on the Integration of Modeling and Control for Automotive systems, 1999.

[3] J. T. Pukrushpan, A. G. Stefanopoulou and H. Peng, *Control of Fuel Cell Power Systems: Principles, Modeling, Analysis and Feedback Design.* , vol. XVII, Springer, 2004, pp. 161.

[4] Moraal, P. and Kolmanovsky, I. (1999). Turbocharger modeling for automotive control applications. *SAE Paper 1999-01-0908.*

[5] Dongsuk Kum, S. Moura, "Plant/Control Optimization of a PEM Hybrid Fuel Cell V2G System," University of Michigan, ME 555, 2007.

[6] California ISO: System Status. http://www.caiso.com/outlook/outlook.html.

[7] Chan-Chiao Lin, Min-Joong Kim, H. Peng and J. W. Grizzle, "System-level model and stochastic optimal control for a PEM fuel cell hybrid vehicle," *Transactions of the ASME. Journal of Dynamic Systems, Measurement and Control,* vol. 128, pp. 878-90, 12. 2006.

[8] H. Peng and George T.C Chiu, "Chapter 9 – Linear Quadratic Optimal Control", in *Design of Digital Control Systems coursepack,* 1994- 2007

[9] S. Pang, J. Farrell, J. Du and M. Barth, "Battery state-of-charge estimation," in *Proceedings of American Control Conference,* 2001, pp. 1644-9.

[10] S. Zhou and J. Shi, "Imbalance estimation for speed-varying rigid rotors using time-varying observer," *Transactions of the ASME. Journal of Dynamic Systems, Measurement and Control,* vol. 123, pp. 637-44, 12. 2001.